SAND2020-5325J

Response of PETN Detonators to Elevated Temperatures

Stephanie A. Coronel*, Michael J. Kaneshige

Sandia National Laboratories, Albuquerque, NM 87185 USA

Abstract

In the present study, commercially available detonators with pentaerythritol tetranitrate (PETN) were subjected to elevated temperatures. The detonators were thermally ignited over a range of heating rates to measure ignition delay time and assess detonator violence. The violence of the detonator was quantified by measuring the velocity of the detonator closure disc (or "flyer"). The maximum flyer velocity of a thermally ignited detonator was comparable in magnitude to that obtained by initiating a room temperature pristine detonator with an exploding bridge wire (under the same confinement); however, the high flyer velocity was not an indication of deflagration to detonation transition (DDT) in the thermally ignited detonator. The detonator responded more violently when initiated at 95% of the ignition delay time of the thermally ignited detonator. Inoperability thresholds were also measured by varying the detonator temperature and the threshold was found to be sensitive at detonator temperatures below the melting point of PETN.

*Corresponding author:
Email address: scorone@sandia.gov (Stephanie A. Coronel)

Keywords:
PETN, PBX 9407, Thermal Ignition, PDV, Detonator

1. Introduction

Assessing the behavior of confined PETN during an accident, such as a fire, is important for safety analysis. In the current study, we investigated the violence of PETN detonators during thermal ignition. We also investigated the success or failure of the PETN detonator to operate as designed after exposure to elevated temperatures. Thermal ignition of a confined explosive occurs when the rate of heat release from exothermic chemical reactions exceeds the rate of heat losses [1]. This process depends on the type of reactant, mass of reactant, reaction rate, pressure, and boundary conditions of the reactant [2]. If the conditions are favorable, it is possible for the thermally ignited explosive to transition from a deflagration to a detonation front. Inoperability refers to whether or not the detonator functions as intended during exposure to elevated temperatures and prior to thermal ignition, after receiving an initiation input. The detonator is deemed operable if it behaves normally, i.e., a detonation front is generated within the explosive after receiving an initiation input, and it is deemed inoperable if a deflagration front is generated within the explosive without a transition to a detonation.

Previous work, shown in Fig. 1, on deflagration to detonation transition (DDT) of confined pristine PETN with a 1200 μm crystal size indicates that a run-to-detonation length, L, or distance from ignition location to location of detonation transition, of at least 15 mm is required; the length

increases for PETN density less than and greater than 70% of the theoretical maximum density (TMD) [3]. Korotkov et al. [4] measured a minimum run-to-detonation length of 20 mm for 80% TMD PETN with a 500 μm crystal size. The minimum run-to-detonation length shifted to 76% TMD for 20 μm crystal size. The shortest run-to-detonation length of 8 mm was measured by Griffiths and Groocock [5] using PETN with a crystal size of 422 μm and 82% TMD. The studies by Luebcke et al. [3] and Korotkov et al. [4] used nominal PETN column diameters of 5 mm and confinement thicknesses of 10 mm (mild steel) and 20 mm (brass and steel), respectively. In contrast, Griffiths and Groocock [5] used a PETN column diameter and confinement thickness of 2.5 mm. The critical detonation diameter for PETN with a crystal size of 100 μm and 240 μm at 56% TMD is 1.5 mm and 3.5 mm, respectively [6]. For completeness, the PETN column was ignited on one end by a flame from lead styphnate in the Griffiths and Groocock [5] experiments. In the Korotkov et al. [4] study the PETN column was ignited on one end by an electrically heated nichrome spiral wire. The Luebcke et al. [3] study used a boron/potassium dichromate mixture to ignite the end of the PETN column. The experimental results shown in Fig. 1 are baseline run-to-detonation lengths of pristine PETN of varying crystal sizes and densities. The run-to-detonation lengths are expected to change for thermally ignited PETN due to changes in porosity after the PETN melts and prior to ignition [7].

This study presents experimental work on sealed commercially available detonators. The detonators were subjected to elevated temperatures to study their response at thermal ignition and operable/inoperable conditions. An

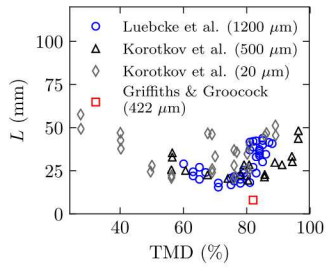

Figure 1: Previous experimental results on deflagration to detonation transition of PETN [3–5].

analysis was performed to determine if DDT occurred in the PETN when thermally ignited at different heating rates. The violence and operability of the detonators was quantitatively assessed by measuring the velocity of the detonator closure disc following initiation. Additionally, the inoperability threshold of the detonator was experimentally determined for a range of detonator surface temperatures. The PETN pellet used in this study was 3.2 mm in length, which is shorter than the lowest experimentally measured run-to-detonation length value of 8 mm [5].

2. Experimental Methodology

Teledyne RISI RP-87 detonators were heated to thermal ignition and also used in inoperability testing. A cross-sectional cut of the cylindrical detonator is shown in Fig. 2. The detonator consists of a low density PETN initiating pellet (23 mg and 0.900 g/cc, 50% TMD) and high-density PBX 9407 (94 wt% RDX, 4 wt% FPC-461 fluoropolymer) output explosive (44 mg and 1.690 g/cc). In all testing, it is the PETN and not the PBX 9407 that is initially thermally ignited or ignited with an exploding bridge wire (EBW);

PETN has a lower ignition temperature than PBX 9407 [8]. The energetic material and header are all contained within a brass sleeve and stainless steel can. In Fig. 2, the closure disc refers to the base of the can, with a thickness of 0.17 ± 0.01 mm adjacent to the PBX 9407 pellet, that detaches in the event of a high-pressure build-up. For the remainder of this paper, the closure disc will be referred to as a "flyer".

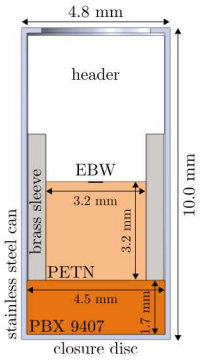

Figure 2: Cross-sectional cut of RP-87 detonator.

The detonator was axially centered in an aluminum cylindrical adapter, shown in Fig. 3; note that the adapter also provides additional confinement for the detonator in the radial direction. The additional confinement does not have an effect on the thermal expansion of the stainless steel can during heating. The linear thermal expansion coefficient of a range of stainless steel types is 17-19 μm/m/K [9]. Considering a temperature range of 300-500 K, the resulting radial expansion of the can will be less than 1 μm; this is 2 orders of magnitude smaller than the space available for expansion between the stainless steel can and aluminum adapter. Figure 3 shows the front and side views, and a cross-sectional cut of two adapter configurations (A and

C); configuration B (not shown in Fig. 3) is the same as configuration A with the addition of a slit for a sapphire window. Each fixture has two feedthroughs for two K-type thermocouple probes (shown as black rods in Fig. 3). Configuration B and C adapters have slits that allow optical access through sapphire windows; the top of each window is aligned with the detonator closure disc. The cross-sectional cut view in Fig. 3 (a) shows two bores (shaded green regions) located along the centerline axis of the adapter and normal to the circumference of the adapter intersecting the centerline axis, respectively; both bores were used for optical access. Each adapter was wrapped by a mineral insulated band heater (Watlow 150 W). To allow for a clear field-of-view through the sapphire window, the band heater was shifted up, off-center, in configurations B and C. By shifting the band heater, one thermocouple feedthrough was blocked; therefore, configurations B and C used a single thermocouple. Each thermocouple was inserted through the feethrough and placed in contact with the detonator surface. The thermocouple closest to the closure disc was used along with a proportional, derivative, integral (PID) controller to heat the adapter at a user-specified heating rate; the difference between the two thermocouple readings was nominally 0.5 K.

Photonic Doppler Velocimetry (PDV) and high-speed imaging were used to measure the flyer response in both thermal ignition and inoperability tests. PDV is a single point diagnostic that measures the velocity of a surface through changes in frequency, i.e., light incident on a moving surface will have a different frequency than the light reflected off of the same surface. 1550 nm laser light was directed at the flyer surface using a GRIN lens fiber collimator (Thorlabs 50-1550A-APC). The reflected light was incident on the

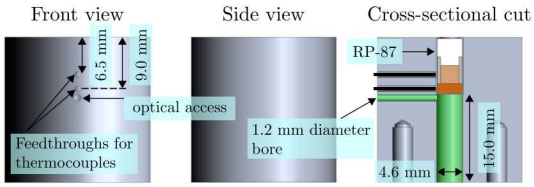

(a) Aluminum cylindrical adapter for RP-87 (configuration A)

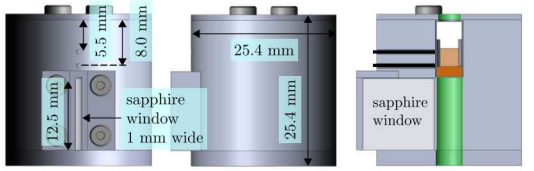

(b) Aluminum cylindrical adapter for RP-87 with slit and slit cover for sapphire window (configuration C)

Figure 3: Front, side, and cross-sectional views of (a) configuration A and (b) configuration C detonator adapters.

same collimator and was interfered with reference light within the PDV system. In the absence of movement of the surface, interference of the reference and reflected light leads to a beat frequency of zero; however, the reference light was modulated to a different frequency such that interference led to a non-zero beat frequency of 4.0-5.5 GHz. The PDV signal was digitized with a Tektronix DPO71254C 12.5 GHZ oscilloscope; a sampling rate of 50 GS/s was used over a test time of 100 μs. A Phantom V2512 high-speed camera was used to image the flyer through the sapphire window at framing rates of 663.265 kfps (configuration B) and 1000 kfps (configuration C) at resolutions of 1088×16 px^2 and 896×16 px^2, respectively.

2.1. Thermal Ignition

Thermal ignition testing was performed with configuration A adapters; only PDV was used as a diagnostic. The PDV oscilloscope was triggered by

the motion of the flyer. Figure 4 shows a 375 nm laser beam (green line) that passes through a 50/50 beam-splitter and is incident on the inside cavity of the detonator adapter. Since the cavity is cylindrical, the beam initially converges after reflection and later diverges; the beam reflects back onto the beam-splitter and is focused on a photodetector. During an ignition event, the flyer moves axially towards the collimator and interrupts the 375 nm laser beam. The interruption is observed by the photodetector as a sharp drop in intensity; this drop in signal serves as a trigger for the PDV system.

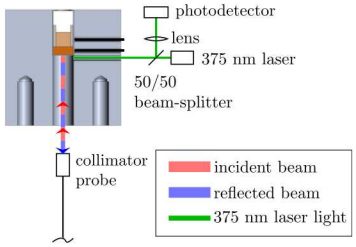

Figure 4: Schematic of thermal ignition PDV oscilloscope trigger setup using configuration A adapter.

2.2. Inoperability

Inoperability testing was performed with the configuration B and C adapters. Both PDV and high-speed imaging were used in configuration C; only high-speed imaging was used with configuration B. After installing a detonator and window in an adapter, the detonator surface was heated to a hold temperature over a time duration of 300 seconds. The detonator was held at that temperature for a specified time (hold time) before sending the arm and fire signal to a Reynolds FS-14 Fireset connected to the detonator EBW leads

to initiate the PETN. The total energy delivered to the EBW was approximately 12 J using a capacitor voltage of 4835 V. When the fire signal was sent, two output signals from a delay generator were also sent to trigger the high-speed camera and PDV oscilloscope.

3. Numerical Methodology

Thermal ignition calculations were performed for the PETN section of the detonator using the conductive energy equation with a chemical source term for the PETN chemistry, shown in Eq. 1.

$$\rho C_b \frac{\partial T}{\partial t} = \nabla \cdot (\lambda \nabla T) + \rho \sum q_i r_i, \tag{1}$$

where C_p, ρ, T, λ, and q_i and r_i are the specific heat, density, temperature, and thermal conductivity of PETN, and the reaction enthalpy and reaction rate of the i^{th} reaction, respectively. The chemistry was modeled with a 4-step mechanism for PETN [10]. The chemical mechanism and associated reaction rates are shown in Table 1 where A: PETN, B: condensed phase intermediates, C: gaseous intermediates, and D: final gaseous products. A_i, E_i, R, and N_j are the pre-exponential factor and activation energy of the i^{th} reaction, universal gas constant, and dimensionless species progress variable of species j, respectively. The chemical kinetic parameters used in Table 1 and reaction enthalpies were taken from Tarver et al. [10]. The thermal parameters for PETN were taken from Lawless et al. [11].

Equation 1 was solved using the method-of-lines in combination with grid refinement and stiff numerical methods and only considering the radial dimension [12].

Mechanism	$\mathrm{A} \xrightarrow{1} \mathrm{B}$, $\mathrm{A} + \mathrm{B} \xrightarrow{2} \mathrm{C}$ $\mathrm{B} \xrightarrow{3} \mathrm{C}$, $\mathrm{C} \xrightarrow{4} \mathrm{D}$
Rates	$r_1 = A_1 \exp\left(-E_1/RT\right) N_\mathrm{A}$ $r_2 = A_2 \exp\left(-E_2/RT\right) N_\mathrm{A} N_\mathrm{B}$ $r_3 = A_3 \exp\left(-E_3/RT\right) N_\mathrm{B}^2$ $r_4 = A_4 \exp\left(-E_4/RT\right) N_\mathrm{C}^2$

Table 1: PETN 4-step mechanism [10].

4. Results

Four series of ignition tests were performed: (a) EBW initiation of the pristine detonator to characterize the flyer velocity, (b) thermal ignition at heating rates, α, of 0.02-0.81 K/s, (c) ramp and initiation tests at nominal heating rates of 0.02, 0.25, and 0.48 K/s, and (d) ramp, hold, and initiation at hold temperatures = {413, 416, 423, 428, 433} K to determine inoperability thresholds. The nominal initial temperature during testing was 298 K.

4.1. Pristine detonator

Figure 5 (a) shows an example PDV signal of a flyer from a EBW initiated pristine detonator (room temperature). An inset shows the PDV signal over a shorter time range. A discrete windowed Fourier Transform was applied to the raw signal using a Hanning window to obtain the spectrogram of Fig. 5 (b); the spectrogram pseudo-color corresponds to relative intensity with units of dB. The dominant frequencies were extracted from the spectrogram to calculate the flyer velocity, $u = \lambda_0 f(t)/2$ where $f(t) = f_d(t) - f_0$, shown in Fig. 5 (c). f is the beat frequency, f_0 and f_d are the frequencies

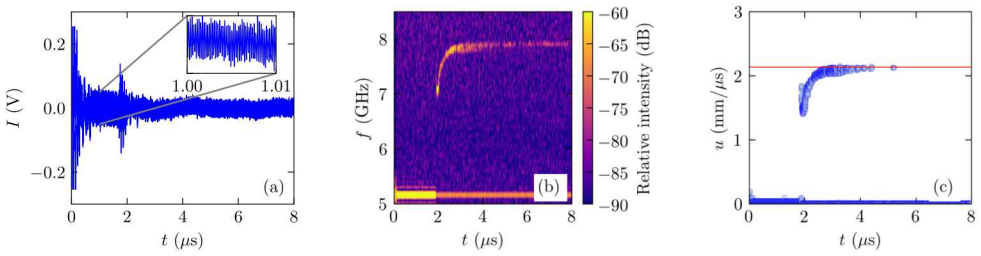

Figure 5: Example of (a) raw PDV signal and corresponding (b) spectrogram; (c) flyer velocity (symbols) calculated from the dominant spectrogram frequencies, the solid red line highlights the final flyer velocity.

of the reference light and Doppler shifted light, respectively, and λ_0 is the laser wavelength. The baseline signal at approximately 5.1 GHz corresponds to back-reflection of the PDV light off of optical elements within the PDV system and does not correspond to motion. Figure 5 (c) indicates that the final velocity of the flyer is 2.140 ± 0.040 mm/μs.

4.2. Thermal ignition

Figure 6 shows the ignition delay time, τ, for RP-87 as a function of the heating rate and detonator surface temperature at ignition, T_{ign}. The ignition delay time is defined as the start of heating to ignition. Figure 6 (a) shows overlap between the experimental and modeling results of τ as a function of α. Figure 6 (b) shows that a variation in ignition temperature of approximately 40 K corresponds to a variation in ignition delay time of almost 2 orders of magnitude. An Arrhenius fit, shown by the solid line in Fig. 6 (b), of the experimental ignition delay times yields an overall activation energy of 98 kJ/mol.

An example flyer velocity profile is shown in Fig. 7 (a) for a heating

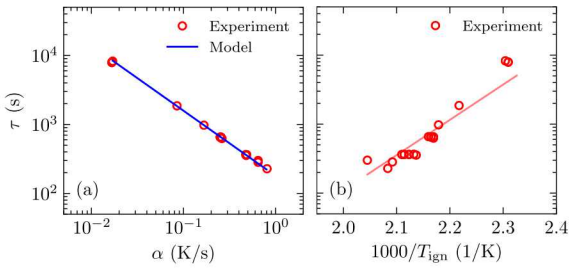

Figure 6: RP-87 ignition delay time as a function of (a) heating rate and (b) inverse ignition temperature.

rate of 0.02 K/s. The flyer reaches a velocity on the order of 2.5 mm/μs approximately 40 μs after initial flyer acceleration. The initial flyer velocity from 0 to 30 μs appears well defined; subsequently, the velocity exhibits significant scatter at the peak and before impacting the PDV collimator probe. The scatter in velocity is either a result of flyer breakup (multiple fragments with a distribution in velocity) and/or tilting of the flyer during its travel that leads to steering of the reflected PDV beam away from the collimator probe. At the peak, the velocity standard deviation is $\sim$ 0.5 mm/μs. Figure 7 (a) also shows the pristine detonator flyer velocity (diamond markers). A comparable peak flyer velocity was achieved by the thermally ignited detonator when compared to the pristine detonator. Recall that it is the PETN in the detonator that ignites and the subsequent reactive front that initiates the PBX 9407 pellet. Since a velocity profile comparable to the one obtained by firing a pristine detonator was not observed in the thermal ignition case, there was no transition to a detonation in the PETN. Figure 7 (b) shows the flyer velocity profiles from all thermal ignition cases; the profiles have been time shifted so that initial flyer movement occurs at

$t_{\text{off}} = 0$ μs. The figure illustrates that there is no effect of the heating rate, ranging from 0.02-0.81 K/s, on the flyer behavior. Figure 8 shows the modeling results of the species progress variable taken at the PETN centerline across heating rates of 0.02-0.81 K/s; time has been normalized by the calculated ignition delay time at each heating rate. The figure shows that immediately before thermal ignition, the PETN is in a similar level of decomposition across the heating rates shown (e.g., $N_{\text{A}} \approx 0.1$ for 0.02-0.81 K/s); therefore, comparable reaction fronts will be generated in the PETN after ignition leading to comparable behavior of the PBX 9407 and flyer across heating rates of 0.02-0.81 K/s.

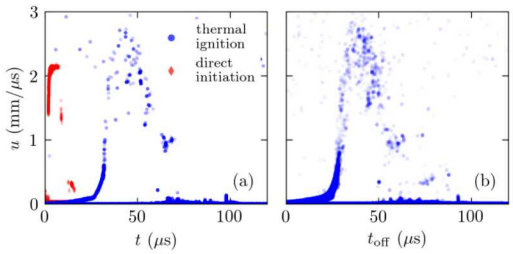

Figure 7: (a) Velocity profiles of a single thermal ignition experiment (circles) and pristine detonator (diamonds); (b) velocity profiles of twelve thermal ignition experiments.

4.3. Ramp and initiate

Ramp and fire tests were performed at heating rates of 0.02, 0.25, and 0.48 K/s and initiated at 95% of the experimental ignition delay time shown Fig. 6 (a). The velocity profiles obtained with PDV are shown in Fig. 9 and have been time shifted so that time to first flyer movement coincides across the three heating rates at $t_{\text{off}} = 0$ μs. In the thermal ignition profiles of Fig. 7,

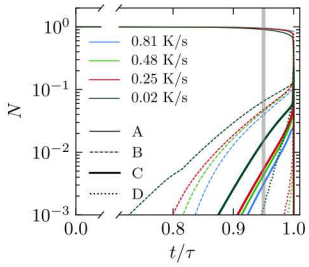

Figure 8: Temporal profiles of calculated species progress variable at PETN centerline; the different line types and colors correspond to different species and heating rates, respectively.

it takes over 20 μs for the flyer to reach a velocity of 0.5 mm/μs, whereas the same velocity is reached in less than 5 μs after initial flyer movement in Figure 9. When firing the detonator at 95% of the ignition delay time, the detonator response will be more violent (higher acceleration) than the response of a thermally ignited detonator at heating rates of 0.02-0.48 K/s. Figure 9 shows that the detonator response is more violent at heating rates of 0.25 and 0.48 K/s than at the lower heating rate of 0.02 K/s. Additionally, the detonator appears to behave similarly at 0.25 K/s and 0.48 K/s; there is overlap in the uncertainty bands across the two velocity profiles. The calculations shown in Fig. 8 indicate that at 95% of the ignition delay time (indicated by the gray vertical line) the species progress variable of PETN, and condensed phase and gaseous intermediates are comparable at heating rates of 0.25 and 0.48 K/s which explains the similar velocity profiles (circle and square markers) shown in Fig. 9. At a heating rate of 0.02 K/s, the PETN has undergone higher levels of decomposition at 95% of the ignition delay time leading to a less violent flyer response (diamond markers in Fig. 9

(b)).

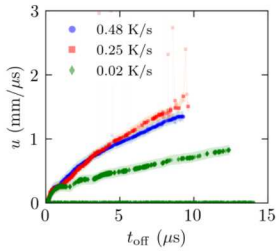

Figure 9: Velocity profiles of flyer response when PETN is EBW initiated at 95% of the ignition delay time: 345 s, 612 s, and 7624 s for heating rates of 0.48 K/s, 0.25 K/s, and 0.02 K/s, respectively; shaded regions correspond to uncertainty bands.

4.4. Ramp, hold, and initiate

Inoperability tests were performed by ramping the detonator external surface to a hold temperature, T_{hold}, over a time duration of 300 seconds and initiating the EBW after a hold time, τ_{hold}. Figure 10 shows a typical temperature profile of the detonator surface to illustrate the ramp, hold, and initiation procedure. For each hold temperature, a number of tests were performed at varying hold times to find the inoperability threshold, i.e., the hold time at which the detonator transitions from operable to inoperable. PDV and high-speed imaging were used in testing to determine if a detonator was operable or inoperable. With PDV, the detonator was deemed operable if the velocity resembled the velocity trace obtained by initiating a pristine detonator (shown in Fig. 5 (c)).

Figure 11 (a) shows images (grayscale represents light intensity) at 1000 kfps using an exposure time of 261 ns of the output of an initiated pristine

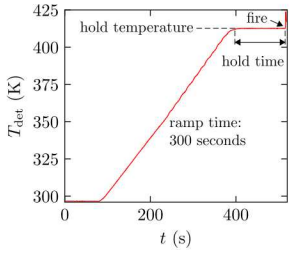

Figure 10: Detonator surface temperature during inoperability testing.

detonator. Each vertical strip corresponds to a field of view 12.5 mm tall and 0.2 mm wide. The strips were stitched next to each other to obtain a plot of space versus time of the flyer. The flyer is located at $z = 0$ mm at time 0 μs and travels from top to bottom after the detonator is initiated. The regions of high intensity correspond to chemiluminescence from the combustion event. The flyer itself is not observed but rather the chemiluminescence trailing it at approximately 3-6 μs. The chemiluminescence entering the field of view at approximately 9 μs is speculated to be expansion of PETN products. An operable test is shown in Fig. 11 (b) using a hold time and temperature of 40 seconds and 416 K, respectively. The same flyer behavior with the trailing chemiluminescence is observed at approximately 3-6 μs indicating an operable detonator. An example of an inoperable detonator is shown in in Fig. 11 (c); chemilumininescence trailing the flyer enters the field of view at 6 μs and reaches the bottom of the field of view after 18 μs.

Figure 12 shows the inoperability results as a function of the hold temperature. The closed and open markers correspond to detonators that detonated and did not detonate, respectively, after applying an initiation input to the EBW. The blue vertical line marks the melting point of PETN (415 K) [13].

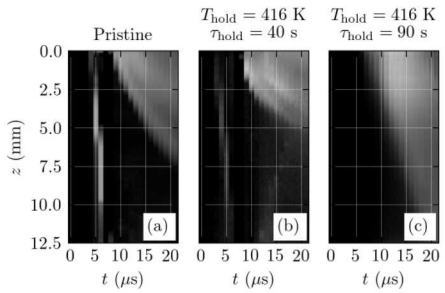

Figure 11: Stitched images of detonator output; (a) pristine detonator, EBW initiated at (b) a hold time 40 seconds and (c) hold time of 90 seconds (hold temperature is 416 K).

The figure shows a sharp jump in the inoperability threshold across the melting point of PETN. Above the melting point, the inoperability threshold is on the order of 20 to 50 seconds. Below the melting point, the inoperability threshold jumps to close to 2000 seconds. At a hold temperature of 433 K the detonator is always inoperable; not shown in the figure is an inoperable point at a hold time of 0 seconds at 433 K.

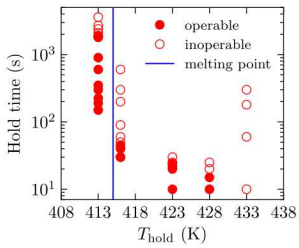

Figure 12: Inoperability results for various hold temperatures; the blue vertical line marks the PETN melting point of 415 K.

Figure 13 shows the inoperability results plotted in terms of the time from trigger to initial flyer movement, τ_f. Initial flyer movement corresponds to

the time when the flyer velocity rises above zero. Not shown in the figure are inoperability results at a hold temperature of 413 K since PDV was not used. Also shown in the figure is a result at a hold temperature of 438 K. The blue horizontal line marks the transition between operable and inoperable at approximately 4 μs. The figure shows that flyer movement is consistently observed at 3.7-4.0 μs in operable cases. This suggests that at operable conditions, the formation of a detonation wave in the PETN following EBW initiation is insensitive to the condition of the PETN; it should be noted that pristine detonators yield τ_f values of 3.6-3.9 μs. Once the detonator becomes inoperable, initial flyer movement occurs at times longer than 4 μs and can be delayed up to 9 μs; the initial flyer movement appears to be more sporadic in the inoperable regime.

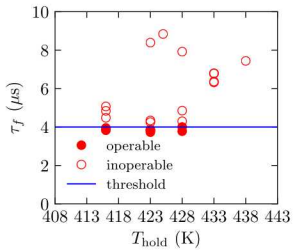

Figure 13: Time to flyer first movement; the blue horizontal line at 4 μs separates the operable and inoperable cases.

The violence of the detonator was assessed at inoperable conditions by fixing the hold time at 300 seconds and varying the hold temperature; this was done over a temperature range of 423-438 K and is shown in Fig. 14. The hold time of 300 seconds is longer than the measured inoperability thresholds shown in Fig. 12. A hold temperature of 443 K was also tested, however,

the PETN thermally ignited before reaching the hold time of 300 seconds. The time to 0.5 mm/μs from initial flyer movement decreases as the hold temperature increases, e.g., it takes approximately 5 μs and 2 μs for the flyer to reach a velocity of 0.5 mm/μs for hold temperatures of 423 K and 425 K, respectively. For hold temperatures of 428-438 K, the flyer accelerates to 0.5 mm/μs in $<<$ 1 μs.

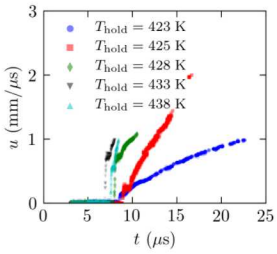

Figure 14: Velocity profiles of flyer response at hold temperatures of 423-438 K and hold time of 300 seconds.

5. Conclusions

In this study, the response of RP-87 detonators to elevated temperatures was investigated via Photonic Doppler Velocimetry and high-speed imaging. A velocity analysis across the heating rates tested (0.02-0.81 K/s) indicated that the flyer response was insensitive to the heating rate when thermally ignited. Additionally, the velocity profiles showed that DDT did not occur in the PETN; however, the flyer still accelerated to a high velocity that was on the same order as the velocity attained by initiating a pristine detonator. Detonators that were heated a various heating rates and then initiated at 95% of the ignition delay time yielded a more violent response than the thermally

ignited detonators. An increase in violence was also observed with an increase in hold temperature in the ramp, hold, and initiate tests with a fixed hold time of 300 seconds. The inoperability thresholds were determined for a range of hold temperatures; the threshold was found to be sensitive at conditions below the melting point of PETN. Finally, a time to flyer first movement of 4 μs was found to separate operable from inoperable detonators.

Acknowledgments

Sandia National Laboratories is a multimission laboratory managed and operated by National Technology & Engineering Solutions of Sandia, LLC, a wholly owned subsidiary of Honeywell International Inc., for the U.S. Department of Energy's National Nuclear Security Administration under contract DE-NA0003525. This paper describes objective technical results and analysis. Any subjective views or opinions that might be expressed in the paper do not necessarily represent the views of the U.S. Department of Energy or the United States Government. We would like to thank our internal reviewer Michael L. Hobbs. We would also like to thank Shane Snedigar and Christopher Colburn for their support in performing the experiments, and Leanna Minier for management support.

References

[1] N. N. Semenov, Chemical Kinetics and Chain Reactions, Oxford University Press, London, 1935.

[2] I. Glassman, Combustion, Elsevier Science & Technology, San Diego, 1996.

[3] P. E. Luebcke, P. M. Dickson, J. E. Field, Journal of Applied Physics 79 (1996) 3499–3503.

[4] A. I. Korotkov, A. A. Sulimov, A. V. Obmenin, V. F. Dubovitskii, A. I. Kurkin, Combustion, Explosion and Shock Waves 5 (1969) 216–222.

[5] N. Griffiths, J. M. Groocock, Journal of the Chemical Society (Resumed) J. Chem. Soc. (1960) 4154–4162.

[6] N. P. Satonkina, Scientific Reports 9 (2019) 12256.

[7] J. L. Maienschein, J. F. Wardell, R. K. Weese, B. J. Cunningham, T. D. Tran, 12th International Detonation Symposium (2002).

[8] P. C. Hsu, S. Strout, J. G. Reynolds, E. M. Kahl, A. Nye, J. Moore, M. McClelland, M. Gresshoff, A. Gash, G. F. Ellsworth, T. E. Heally, 16th International Detonation Symposium (2018).

[9] J. W. Elmer, D. L. Olson, D. K. Matlock, Welding Journal 61 (1982) 293s–301s.

[10] C. Tarver, T. Tran, R. Whipple, Propellants, Explosives, Pyrotechnics 28 (2003) 189–193.

[11] Z. D. Lawless, M. L. Hobbs, M. J. Kaneshige, Journal of Energetic Materials 38 (2020) 214–239.

[12] R. J. Gross, M. R. Baer, M. L. Hobbs Sandia Report (1993) SAND93–1603.

[13] M. L. Hobbs, W. B. Wente, M. J. Kaneshige, The Journal of Physical Chemistry A J. Phys. Chem. A 114 (2010) 5306–5319.